Journal of Materials Chemistry C

PAPER

View Article Online
View Journal | View Issue

Cite this: J. Mater. Chem. C, 2019, 7, 8383

In situ encapsulation of pyridine-substituted tetraphenylethene cations in metal–organic framework for the detection of antibiotics in aqueous medium†

Yan-Mei Ying,[a] Chen-Lei Tao,[a] Maoxing Yu,[b] Yi Xiong,[b] Chang-Rui Guo,[a] Xun-Gao Liu *[a] and Zujin Zhao*[b]

Received 26th April 2019,
Accepted 6th June 2019

DOI: 10.1039/c9tc02229e

rsc.li/materials-c

Antibiotics have become a pollutant in water due to their abuse, which poses a threat to the environment and human health. An urgent and meaningful task is to develop highly sensitive and selective sensors. Herein, a new and simple luminescent MOF $[Zn_8(C_5H_4N_5)_4(C_{14}H_8O_4)_6O(C_{50}H_{44}N_4)_{0.5}]$ (TMPyPE@bio-MOF-1) was synthesized by *in situ* encapsulation of cationic TPE-based guest TMPyPE into an anionic MOF. TMPyPE@bio-MOF-1 exhibits high stability and strong fluorescence in water, and can selectively and sensitively detect nitrofuran antibiotics in aqueous medium. At the same titration concentration, TMPyPE@bio-MOF-1 shows higher fluorescence quenching efficiencies of 96% for NFZ and 95.5% for NFT compared with other antibiotics, which can be detected by the naked eye. Due to the simplicity and sensitivity of analysis, the tetraphenylethene-based luminogen encapsulated LMOF material reported would have wide application potential in environmental pollution analysis.

Introduction

Antibiotics play an important role in improving human health, and preventing and treating infections of animals and plants. However, with the increasing use of antibiotics, they have become well-known water pollutants. As a kind of effective antibiotic, nitrofuran antibiotics (NFAs) were once used to treat bacterial infections in food-producing animals due to their low cost and good efficacy. The residuals of NFAs as well as metabolites discharged from agricultural runoff and wastewater treatment plants have high potential to enter surface and ground waters. Thus, developing highly sensitive and selective sensors for NFAs is an urgent and meaningful task. So far, some techniques such as liquid chromatography-mass spectrometry (LC-MS), gas chromatography-mass spectrometry (GC-MS), micellar electrokinetic capillary chromatography (EC), *etc.* have been used to detect trace amounts of antibiotics.[1–6] But fluorescence based chemical sensing is considered as one of the most competitive methods among the proposed techniques because of its economic feasibility, high-efficiency, and convenient and simple operation. Fluorescent materials that show responses towards antibiotics are essential for the fluorescence-based method. Recently, a few luminescent metal–organic frameworks (LMOFs) have been reported for the detection of antibiotics.[7,8]

Tetraphenylethene (TPE), as one of the most popular aggregation-induced emission (AIE) luminogens, has been successfully used to construct novel porous framework materials, such as luminescent MOFs,[9–11] covalent organic frameworks (COFs),[12,13] porous organic polymers (POPs),[14–16] and other functional optoelectronic materials for applications in organic light-emitting diodes,[17–19] fluorescent chemical sensors,[20–22] and biological probes.[23–25] In terms of building TPE-based luminescent MOFs, the common strategy is to introduce carboxylic acid or pyridine coordination groups on TPE as multidentate ligands, which can chelate metal ions to form the frameworks.[26–29] It is very convenient that TPE-based luminogens can be encapsulated into known MOFs, which can also avoid determining their single crystal structures. Due to their unique tunnel structures, MOFs are emerging as valuable host matrices capable of encapsulating cationic dyes,[30,31] quantum dots,[32,33] nanoparticles,[34–36] and small luminous molecules[37] for manipulating their photophysical properties, or sensing, separation or catalysis purposes. However, so far, it is still

[a] College of Material, Chemistry and Chemical Engineering, Hangzhou Normal University, Hangzhou 310036, China. E-mail: xungaoliu@hznu.edu.cn
[b] State Key Laboratory of Luminescent Materials and Devices, Center for Aggregation-Induced Emission, South China University of Technology, Guangzhou 510640, China. E-mail: mszjzhao@scut.edu.cn

† Electronic supplementary information (ESI) available: Experimental details, thermal analysis, emission spectra, ^{1}H NMR spectra, PXRD patterns and luminescence sensing. See DOI: 10.1039/c9tc02229e

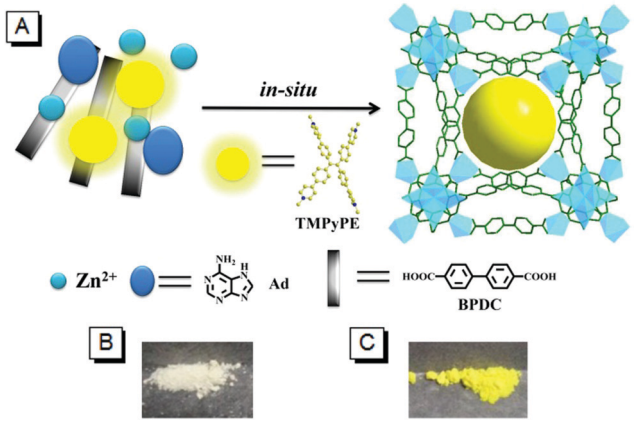

Fig. 1 (A) Schematic illustration of the encapsulation of TMPyPE into bio-MOF-1. Change of colours before (B) and after (C) encapsulation.

difficult to obtain luminescent MOFs with high fluorescence quantum yields *via* encapsulating common luminescent guest molecules into MOFs. Introducing AIE-active guests, such as TPE, should be a wise method to address this issue. However, to the best of our knowledge, there are few successful reports about encapsulating TPE-based guests into MOFs.

Inspired by our previous reported TPE-based luminescent MOFs for sensing antibiotics and nitro aromatic vapors,[38–40] herein, anionic bio-MOF-1 is used as a scaffold for encapsulation of strongly emitting tetrakis[4-(1-methylpyridin-4-yl)phenyl]ethene iodide (TMPyPE iodide) to get the TMPyPE@bio-MOF-1 composite ($[Zn_8(C_5H_4N_5)_4(C_{14}H_8O_4)_6O(C_{50}H_{44}N_4)_{0.5}]$). As depicted in Fig. 1, cationic TMPyPE molecules are incorporated into bio-MOF-1 based on *in situ* encapsulation, which requires short processing times and successfully makes the guest molecules unable to escape because of the strong electrostatic interactions.[41,42] Despite the fact that there are many reported examples of TPE-based MOFs, this is a novel strategy to obtain highly luminescent MOFs with AIE guests *via* a very simple and one-step process. Based on the outstanding stability in water of activated TMPyPE@bio-MOF-1, the selective and sensitive detection of NFA in water is realized.

Experimental section

Synthesis of tetrakis[4-(1-methylpyridin-4-yl)phenyl]ethene iodide (TMPyPE iodide)

The synthesis of TMPPE iodide was carried out according to the literature method.[43] An amount of 0.25 mL of CH_3I was added to a solution of 100 mg of 1,1,2,2-tetrakis(4-(pyridin-4-yl)phenyl)-ethane (TPyPE) in a mixed solution of acetonitrile (7.5 mL) and DMF (7.5 mL) dropwise by an injector, under a nitrogen atmosphere. The solution was then stirred for 24 h at room temperature. After removing acetonitrile under vacuum, the iodide salt was precipitated from DMF by adding Et_2O, filtered, and washed with Et_2O. The precipitate was dried under vacuum, giving the yellow product (85% yield). ^{1}H NMR (500 MHz, DMSO-d_6, TMS, ppm, Fig. 2A): δ = 8.99 (d, J = 6.9 Hz, 8H), 8.44 (d, J = 7.0 Hz, 8H), 7.98 (d, J = 8.5 Hz, 8H), 7.39 (d, J = 8.4 Hz, 8H), 4.32 (s, 12H).

Synthesis of TMPyPE@bio-MOF-1

The synthesis of TMPyPE@bio-MOF-1 *via* a solvothermal reaction was modified from the original reported procedures.[44] To a solution of adenine (0.125 mmol), 4,4′-biphenyl dicarboxylic acid (BPDC) (0.25 mmol) in DMF (13.5 mL) was added with zinc acetate dihydrate (0.375 mmol). After adding nitric acid (1 mmol), it becomes a clear solution. Then, TMPyPE iodide (0.016 mmol) and water (0.5 mL) were added to the clear solution. The vial was capped and the resulting solution was heated at 130 °C for 24 h to afford the yellow powder product. The product was collected, washed with DMF and methanol several times and dried in air. IR (KBr pellet, cm^{-1}, Fig. S6, ESI†): 3334 (s), 3191 (s), 1659 (s), 1606 (s), 1544 (s), 1470 (w), 1383 (s), 1214 (w), 1176 (w), 1155 (w), 1102 (w), 1006 (w), 841 (m), 771 (s), 683 (m).

Synthesis of activated TMPyPE@bio-MOF-1

As-synthesized TMPyPE@bio-MOF-1 was soaked in fresh CH_2Cl_2 at room temperature for three days to completely remove the DMF solvent molecules. During this time, the organic solvent was removed and replenished with fresh CH_2Cl_2 every 24 h. After solvent exchange was completed, the compound was dried at 60 °C under high vacuum for 6–7 h to

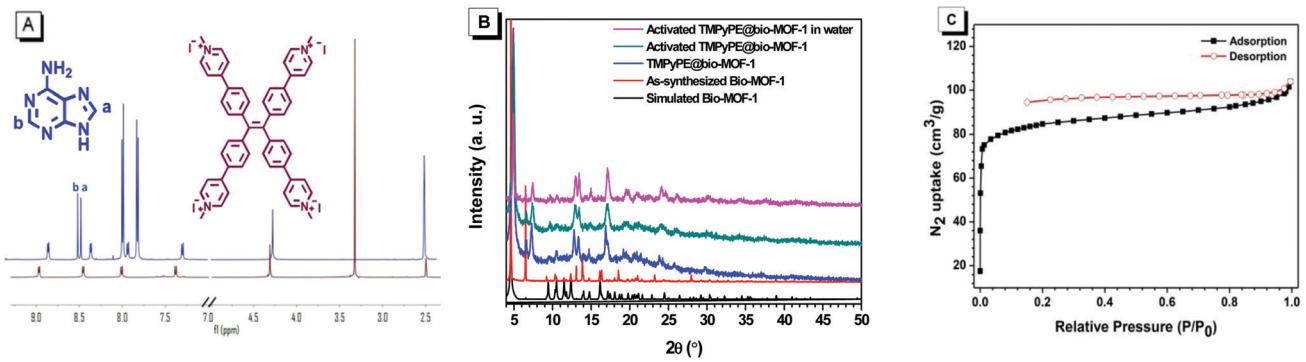

Fig. 2 (A) ^{1}H-NMR spectra for TMPyPE iodide (red) and TMPyPE@bio-MOF-1 (blue). (B) PXRD patterns of simulated Bio-MOF-1 (black), as-synthesized Bio-MOF-1 (red), TMPyPE@bio-MOF-1 (blue), activated TMPyPE@bio-MOF-1 (green) and activated TMPyPE@bio-MOF-1 after being soaked in water (pink), respectively. (C) N_2 adsorption isotherms (77 K) for activated TMPyPE@bio-MOF-1.

get the desolvated sample. ^{1}H NMR (500 MHz, DMSO-d_6, D_2SO_4, TMS, ppm, Fig. 2A): δ = 8.85 (d, J = 6.9 Hz, 1H), 8.51 (s, 8H), 8.47 (s, 1H), 8.36 (d, J = 6.9 Hz, 1H), 7.99 (d, J = 8.3 Hz, 6H), 7.93 (d, J = 8.4 Hz, 1H), 7.82 (d, J = 8.4 Hz, 6H), 7.29 (d, J = 8.3 Hz, 1H), 4.26 (s, 2H).

Procedure for sensing experiments

A water suspension of activated TMPyPE@bio-MOF-1 (0.5 mg mL^{-1}) was utilized to detect different kinds of antibiotics. Fluorescence was measured by adding different amounts of antibiotics (1 mM) to the suspension of activated TMPyPE@bio-MOF-1, and the emission spectra were recorded on a PerkinElmer LS55 spectrofluorometer. Before each fluorescence measurement, the suspension was vortexed for 30 seconds to form a homogeneous phase. The emission spectra were obtained at an excitation wavelength of 365 nm, and the slit widths of both the source and the detector for the excitation and the emission were maintained at 10 nm to maintain consistency. The quenching efficiency (%) was defined by $(I_0 - I)/I_0 \times 100\%$, where I_0 and I are the fluorescence intensities of the activated TMPyPE@bio-MOF-1 suspension before and after the addition of antibiotics, respectively.

pH stability test

Activated TMPyPE@bio-MOF-1 was soaked in HCl and NaOH aqueous solutions (10^{-3} M, 10^{-6} M, 10^{-5} M) with PH values of 3, 6 and 9 for 3 h. After that, processed TMPyPE@bio-MOF-1 was characterized by PXRD.

Results and discussion

Characterization and structure of TMPyPE@bio-MOF-1

Bio-MOF-1 is a crystalline porous material with 1D channels in which $Me_2NH_2^+$ cations reside as counterions (Fig. 1). Anionic Bio-MOF-1 can permit the entrance of cationic TMPyPE into the channels by electrostatic attraction. It is obvious that TMPyPE is enriched into the pores of bio-MOF-1 from the solution as evidenced by the contrasting colors of white and yellow under daylight (Fig. 1). The structure of synthesized TMPyPE@bio-MOF-1 was investigated by ^{1}H-NMR, Powder X-ray diffraction (PXRD) analysis, as shown in Fig. 2, and scanning electron microscopy (SEM), as shown in Fig. S4 (ESI†). The ^{1}H-NMR spectrum obtained after dissolving thermally activated TMPyPE@bio-MOF-1 (at 333 K under vacuum for 7 h) (Fig. 2A and Fig. S1, ESI†) shows two doublets of 4,4′-biphenyl dicarboxylic acid (7.99 and 7.82 ppm; 12H), and the signals of two protons of the adenine ring (8.51 and 8.47 ppm; 2H). As expected, based on the structural formula of bio-MOF-1 ($[Zn_8(ad)_4(BPDC)_6O\cdot 2Me_2NH_2^+]$), the ratio of adenine to BPDC is 2 : 3. After the cationic TMPyPE molecules are encapsulated in bio-MOF-1, this ratio remains identical, indicating that the resulting structure is consistent with that of bio-MOF-1. PXRD patterns of TMPyPE@bio-MOF-1 and activated TMPyPE@bio-MOF-1 are similar to that of bio-MOF-1 as well as the simulated PXRD pattern, which further validates their structural consistency and good stability after solvent removal. Based on the partial enlargement of Fig. 2B, we can see that there is an additional peak between 7° and 8° which does not appear in the simulated and as-synthesized Bio-MOF-1 curve (Fig. S3, ESI†). This is probably due to the encapsulation of TMPyPE. Due to the strong electrostatic interactions between cationic TMPyPE and the anionic framework, it is not easy for the encapsulated TMPyPE cations to escape in DMF or water (Fig. S9, ESI†). The excellent water stability of bio-MOF-1 has been fully confirmed in the literature.[44] Indeed, activated TMPyPE@bio-MOF-1 also shows good stability in water as evidenced by PXRD experiments (Fig. 2B). At the same time, the pH stability has been studied (Fig. S3, ESI†). The PXRD patterns show that the material exhibits stability after being soaked in HCl and NaOH aqueous solutions with PH values of 3, 6 and 9.

The thermal stability of TMPyPE@bio-MOF-1 has been examined by thermogravimetric analysis (TGA) in nitrogen (Fig. S5, ESI†). It was observed that the first weight loss of 17% is attributable to the evaporation of physisorbed DMF (30–200 °C). Then, a significant weight loss of 50% in the temperature range of 400–650 °C occurs due to the structural breakdown of BPDC (m.p. above 300 °C) and adenine (m.p. 360–365 °C). A stable plateau from 30 to 400 °C is observed on the thermogravimetric curve of activated TMPyPE@bio-MOF-1, indicating the complete removal of its solvent molecules and that the thermal stability is as high as 400 °C.

To verify the permanent porosity, N_2 adsorption–desorption measurements at 77 K for activated TMPyPE@bio-MOF-1 were performed (Fig. 2C). As expected, the Brunauer–Emmett–Teller specific surface area of activated TMPyPE@bio-MOF-1 is 264.1 m^2 g^{-1}, which is smaller than that of bio-MOF-1 ($\sim$1700 m^2 g^{-1}) due to the presence of the TMPyPE guest.[44]

Luminescence properties of TMPyPE@bio-MOF-1

The solid-state fluorescence behaviours of bio-MOF-1, TMPyPE, TMPyPE@bio-MOF-1 and activated TMPyPE@bio-MOF-1 were investigated at room temperature. The solid-state fluorescence spectrum of as-synthesized bio-MOF-1 shows bright blue fluorescence at 384 nm while TMPyPE shows strong yellow emission at 602 nm (λ_{ex} = 300 nm, Fig. S7, ESI†). As shown in Fig. S8 (ESI†), upon excitation at 365 nm, TMPyPE@bio-MOF-1 displays a strong emission peak at 522 nm, while the emission peak of activated TMPyPE@bio-MOF-1 is red-shifted to 547 nm, possibly due to the increased electronic coupling between the encapsulated TMPyPE cations.[45] The absolute fluorescence quantum yields (Φ_Fs) of TMPyPE@bio-MOF-1 and activated TMPyPE@bio-MOF-1 are 78.5% and 77.3%, respectively, measured by an integrating sphere, being much higher than those of many TPE-based MOFs.[46,47] At the same time, the fluorescence lifetimes (τs) are 3.3 ns and 3.2 ns for TMPyPE@bio-MOF-1 and activated TMPyPE@bio-MOF-1, respectively, which agree well with the tendency of the Φ_Fs. The Φ_F and τ of TMPyPE@bio-MOF-1 are much larger than those of TMPyPE (Φ_F = 1.37%, τ = 1.37 ns) in solid form, which can be attributed to the more efficient blockage of the radiationless channel by the greatly rigidified molecular structure in the confined crystalline framework.[48,49]

Antibiotic sensing performance of TMPyPE@bio-MOF-1

Considering its high stability and strong emission in aqueous solution, TMPyPE@bio-MOF-1 can be used as a fluorescent sensor for detecting antibiotics in aqueous medium. A total of ten frequently used water-soluble antibiotics from seven classes, nitrofurans (nitrofurantoin, NFT; nitrofurazone, NFZ), nitroimidazoles (metronidazole and MDZ), chloramphenicols (chloramphenicol and CAP), sulfonamides (sulfathiazole, STZ; sulfadiazine, SDZ; sulfamethazine, SMZ), quinolones (norfloxacin, NFX), macrolides (erythromycin and EM), and β-lactams (amoxicillin and AMX), were investigated. The finely ground sample of activated TMPyPE@bio-MOF-1 was dispersed in water to detect these antibiotics. As shown in Fig. 3, although different degrees of fluorescence quenching of activated TMPyPE@bio-MOF-1 are obtained upon the addition of an identical amount of antibiotics, NFZ and NFT exhibit the most significant fluorescence quenching efficiencies of 96.0% and 95.5%, respectively, at 1 mM (370 μL) analyte concentration (Fig. 3). However, the fluorescence quenching efficiencies of other antibiotics are less than 30% under the same conditions. This clearly demonstrates the high selectivity of activated TMPyPE@bio-MOF-1 towards NFZ and NFT over all the antibiotic analytes. Furthermore, the fluorescence quenching effect can be quantitatively rationalized by the Stern–Volmer equation, $I_0/I = 1 + K_{SV}[M]$,[50] where K_{SV} is the quenching constant (M^{-1}), [M] is the molar concentration of the analyte, and I_0 and I are the emission intensities before and after the addition of the analyte. The Stern–Volmer (SV) plots for the antibiotic aqueous solutions shown in Fig. S14 (ESI†) more intuitively demonstrate the high selectivity of activated TMPyPE@bio-MOF-1 to NFZ and NFT. As shown in Fig. S10 (ESI†), the K_{SV} value is calculated as $4.48 \times 10^4\ M^{-1}$ for NFZ and $4.42 \times 10^4\ M^{-1}$ for NFT, revealing a strong quenching effect. Based on the IUPAC criteria ($3\sigma/K_{SV}$),[51] the limits of detection (LODs) for NFZ and NFT are estimated to be 0.110 and 0.134 ppm, respectively, which are comparable to the value of 0.1 ppm for the previously reported TPE-based luminescent MOF.[40] The detection limits were further confirmed by the fluorescence titrations of NFZ and NFT at low concentrations (Fig. S11 and S12, ESI†). This proves the high sensitivity for selective NFA detection in aqueous medium, extremely important for environmental monitoring. The change in the luminescence response for activated TMPyPE@bio-MOF-1 towards NFZ and NFT can also be markedly well distinguished under 365 nm UV irradiation (Fig. 3). In addition, activated TMPyPE@bio-MOF-1 can be reused by centrifuging the suspension and washing several times with water.

Sensing mechanism

In order to understand the fluorescence quenching effect of TMPyPE@bio-MOF-1 towards NFAs, the quenching mechanism was investigated. After immersing in NFZ or NFT aqueous solution, the structure of TMPyPE@bio-MOF-1 remains unchanged,

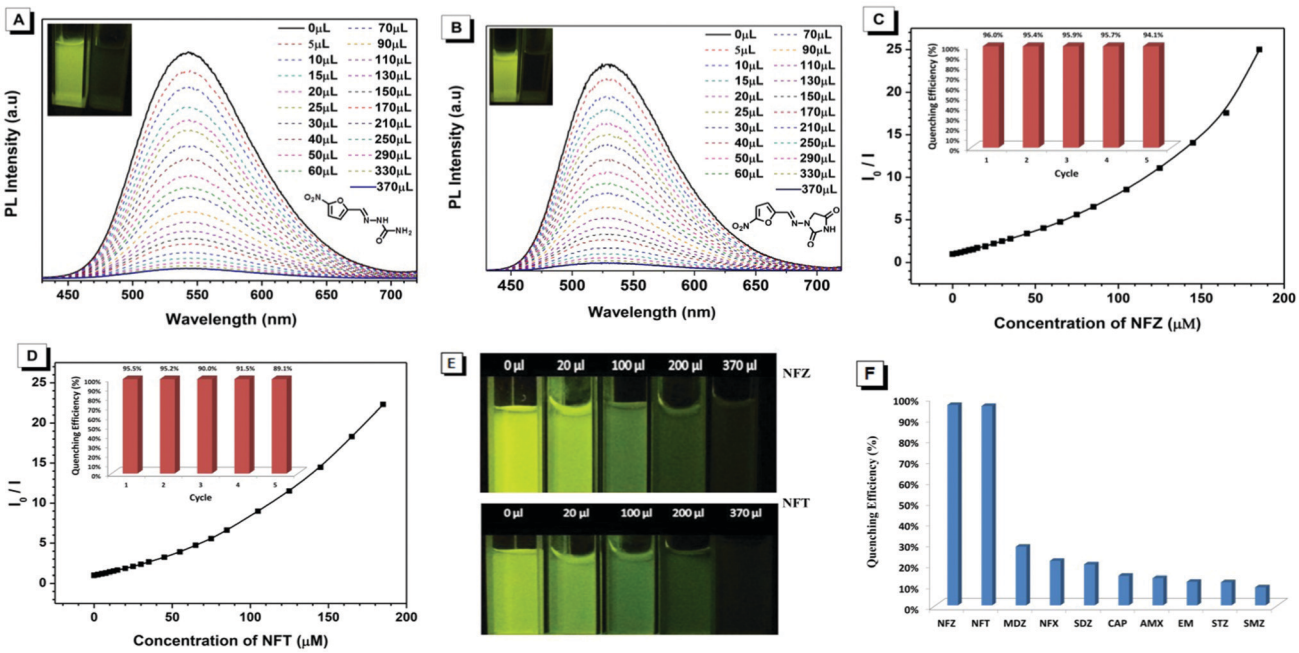

Fig. 3 (A) Emission spectra of activated TMPyPE@bio-MOF-1 suspension upon addition of nitrofurazone (NFZ) aqueous solution (1 mM). (B) Emission spectra of activated TMPyPE@bio-MOF-1 suspension upon addition of nitrofurazone (NFT) aqueous solution (1 mM). (C) Plots of I_0/I *vs.* NFZ concentration in aqueous solution for activated TMPyPE@bio-MOF-1. Inset: Quenching efficiencies of activated TMPyPE@bio-MOF-1 in recyclable experiments for NFZ. (D) Plots of I_0/I *vs.* NFT concentration in aqueous solution for activated TMPyPE@bio-MOF-1. Inset: Quenching efficiencies of activated TMPyPE@bio-MOF-1 in recyclable experiments for NFT. (E) Fluorescence photos of activated TMPyPE@bio-MOF-1 aqueous suspension with gradually increased NFZ and NFT. (F) Percentage of fluorescence quenching of activated TMPyPE@bio-MOF-1 using different antibiotics (1 mM, 370 μL) at room temperature (λ_{ex} = 365 nm).

which can be confirmed by PXRD (Fig. S15, ESI†). Since the UV-vis absorption spectra of antibiotics are basically not overlapped with the emission spectra of activated TMPyPE@bio-MOF-1, the fluorescence resonance energy transfer (FRET) may hardly contribute to the fluorescence quenching (Fig. S16, ESI†). However, the strong adsorption of NFZ and NFT near the excitation wavelength (365 nm), which might effectively suppress the excitation energy absorption of TMPyPE@bio-MOF-1, could be the main cause of fluorescence quenching.[52] To verify this guess, the fluorescence responses of TMPyPE@bio-MOF-1 to NFZ and NFT were detected at the excitation of 440 nm, which was outside the range of NFZ and NFT strong absorption (Fig. S17, ESI†). As expected, the K_{SV} values were calculated as 1.62×10^4 M^{-1} for NFZ and 1.45×10^4 M^{-1} for NFT at 440 nm excitation, which were much less than those at 365 nm excitation (4.48×10^4 M^{-1} for NFZ and 4.42×10^4 M^{-1} for NFT). Another possible fluorescence quenching mechanism is photon-induced electron transfer (PET).[38–40] To examine the possibility of this process, the HOMO and LUMO energy levels of NFZ, NFT and TMPyPE were calculated by using the density functional theory (DFT) method. The LUMO energy level of TMPyPE (−10.35 eV) is lower than that of NFZ (−2.65 eV) and NFT (−2,83 eV), which cannot support the PET from TMPyPE to NFZ and NFT (Fig. S18, ESI†). However, the HOMO energy level of TMPyPE (−13.44 eV) is also lower than that of NFZ (−6.61 eV) and NFT (−6.38 eV), which makes it possible for the transfer of electrons from the HOMO of NFZ and NFT to the HOMO of excited TMPyPE. So, the observed fluorescence quenching may involve electron transfer from NFZ and NFT to TMPyPE.[53,54] In conclusion, both the strong absorption of NFZ and NFT at the excitation wavelength (365 nm) and the reductive electron transfer may be the main reasons for fluorescence quenching.

Conclusions

In summary, a responsive composite, $[Zn_8(C_5H_4N_5)_4(C_{14}H_8O_4)_6O(C_{50}H_{44}N_4)_{0.5}]$ (TMPyPE@bio-MOF-1), has been successfully synthesized by *in situ* encapsulating a pyridine-substituted TPE cation, TMPyPE, within anionic bio-MOF-1. TMPyPE@bio-MOF-1 and activated TMPyPE@bio-MOF-1 exhibit high Φ_Fs of 78.5% and 77.3%, respectively. Activated TMPyPE@bio-MOF-1 shows higher fluorescence quenching efficiencies of 96% for NFZ and 95.5% for NFT as compared with other antibiotics at the same titration concentration and low detection limits of 0.110 ppm for NFZ and 0.134 ppm for NFT, respectively, indicating excellent selective and sensitive detection of NFAs in the water phase. As far as we know, it is the first example of a LMOF obtained by *in situ* encapsulation of TPE derivative cations. Due to the preparation simplicity and fluorescence sensitivity towards antibiotics, the novel luminescent MOF could have wide application potential in environmental pollution control.

Conflicts of interest

There are no conflicts to declare.

Acknowledgements

We gratefully acknowledge the National Natural Science Foundation of China (21788102 and 21671051), the Zhejiang Provincial Natural Science Foundation of China (LY15B010006), the Pandeng Plan Foundation of Hangzhou Normal University for Youth Scholars of Materials, Chemistry and Chemical Engineering and the National Undergraduate Training Program for Innovation and Entrepreneurship for the financial support.

Notes and references

1 D. Fatta, A. Nikolaou, A. Achilleos and S. Meric, *Trends Anal. Chem.*, 2007, **26**, 515.
2 T. A. Ternes, M. Bonerz, N. Herrmann, D. Löffler, E. Keller, B. B. Lacida and A. C. Alder, *J. Chromatogr. A*, 2005, **1067**, 213.
3 W. M. A. Niessen, *J. Chromatogr. A*, 1998, **812**, 53.
4 A. L. Batt and D. S. Aga, *Anal. Chem.*, 2005, **77**, 2940.
5 Y.-Q. Hong, X. Guo, G.-H. Chen, J.-W. Zhou, X.-M. Zou, X. Liao and T. Hou, *J. Food Saf.*, 2018, **38**, e12382.
6 P. U. Wickramanayake, T. C. Tran, J. G. Hughes, M. Macka, N. Simpson and P. J. Marriott, *Electrophoresis*, 2006, **27**, 4069.
7 N. Xu, Q. Zhang, B. Hou, Q. Cheng and G. Zhang, *Inorg. Chem.*, 2018, **57**, 13330.
8 F. Zhang, H. Yao, Y. Zhao, X. Li, G. Zhang and Y. Yang, *Talanta*, 2017, **174**, 660.
9 X.-X. Wu, H.-R. Fu, M.-L. Han, Z. Zhou and L.-F. Ma, *Cryst. Growth Des.*, 2017, **17**, 6041.
10 Q.-Y. Li, Z. Ma, W.-Q. Zhang, J.-L. Xu, W. Wei and H. Lu, *Chem. Commun.*, 2016, **52**, 11284.
11 F. Wang, W. Liu, S. J. Teat, F. Xu, H. Wang, X. Wang, L. An and J. Li, *Chem. Commun.*, 2016, **52**, 10249.
12 H. Ding, J. Li, G. Xie, G. Lin, R. Chen, Z. Peng, C. Yang, B. Wang, J. Sun and C. Wang, *Nat. Commun.*, 2018, **9**, 5234.
13 Q. Gao, X. Li, G.-H. Ning, H.-S. Xu, C. Liu, B. Tian, W. Tang and K. P. Loh, *Chem. Mater.*, 2018, **30**, 1762.
14 Q. Zhao and Y. Liu, *Chem. Commun.*, 2018, **54**, 6068.
15 X. Li, Z. Li and Y.-W. Yang, *Adv. Mater.*, 2018, **30**, 1800177.
16 E. Preis, W. Dong, G. Brunklaus and U. Scherf, *J. Mater. Chem. C*, 2015, **3**, 1582.
17 L. Chen, G. Lin, H. Peng, H. Nie, Z. Zhuang, P. Shen, S. Ding, D. Huang, R. Hu, S. Chen, F. Huang, A. Qin, Z. Zhao and B. Z. Tang, *J. Mater. Chem. C*, 2016, **4**, 5241.
18 L. Chen, Y. Jiang, H. Nie, R. Hu, H. S. Kwok, F. Huang, A. Qin, Z. Zhao and B. Z. Tang, *ACS Appl. Mater. Interfaces*, 2014, **6**, 17215.
19 B. Chen, B. Liu, J. Zeng, H. Nie, Y. Xiong, J. Zou, H. Ning, Z. Wang, Z. Zhao and B. Z. Tang, *Adv. Funct. Mater.*, 2018, **28**, 1803369.
20 R. X. Zhang, P. F. Li, W. J. Zhang, N. Li and N. Zhao, *J. Mater. Chem. C*, 2016, **4**, 10479.
21 Y. Chen, W. Zhang, Y. Cai, R. T. K. Kwok, Y. Hu, J. W. Y. Lam, X. Gu, Z. He, Z. Zhao, X. Zheng, B. Chen, C. Gui and B. Z. Tang, *Chem. Sci.*, 2017, **8**, 2047.
22 X. Huang, H. Zhoua, Y. Huang, H. Jiang, N. Yang, S. A. Shahzad, L. Meng and C. Yu, *Biosens. Bioelectron.*, 2018, **121**, 236.

23 X. Yang, N. Wang, L. Zhang, L. Dai, H. Shao and X. Jiang, *Nanoscale*, 2017, **9**, 4770.
24 X. He, X. Wang, L. Zhang, G. Fang, J. Liu and S. Wang, *Sens. Actuators, B*, 2018, **271**, 289.
25 Y. Chen, X. Min, X. Zhang, F. Zhang, S. Lu, L.-P. Xu, X. Lou, F. Xia, X. Zhang and S. Wang, *Biosens. Bioelectron.*, 2018, **111**, 124.
26 Z. Wei, Z.-Y. Gu, R. K. Arvapally, Y.-P. Chen, R. N. McDougald, Jr., J. F. Ivy, A. A. Yakovenko, D. Feng, M. A. Omary and H.-C. Zhou, *J. Am. Chem. Soc.*, 2014, **136**, 8269.
27 B. J. Deibert, E. Velasco, W. Liu, S. J. Teat, W. P. Lustig and J. Li, *Cryst. Growth Des.*, 2016, **16**, 4178.
28 Z. Hu, W. P. Lustig, J. Zhang, C. Zheng, H. Wang, S. J. Teat, Q. Gong, N. D. Rudd and J. Li, *J. Am. Chem. Soc.*, 2015, **137**, 16209.
29 W. P. Lustig, F. Wang, S. J. Teat, Z. Hu, Q. Gong and J. Li, *Inorg. Chem.*, 2016, **55**, 7250.
30 X.-L. Hu, C. Qin, X.-L. Wang, K.-Z. Shao and Z.-M. Su, *Chem. Commun.*, 2015, **51**, 17521.
31 J. Yu, Y. Cui, H. Xu, Y. Yang, Z. Wang, B. Chen and G. Qian, *Nat. Commun.*, 2013, **4**, 2719.
32 D. Zhang, Y. Xu, Q. Liu and Z. Xia, *Inorg. Chem.*, 2018, **57**, 4613.
33 J. Ren, T. Li, X. Zhou, X. Dong, A. V. Shorokhov, M. B. Semenov, V. D. Krevchik and Y. Wang, *Chem. Eng. J.*, 2019, **358**, 30.
34 J. Chen, H. Chen, T. Wang, J. Li, J. Wang and X. Lu, *Anal. Chem.*, 2019, **91**, 4331.
35 J. Wang, H. Chen, F. Ru, Z. Zhang, X. Mao, D. Shan, J. Chen and X. Lu, *Chem. – Eur. J.*, 2018, **24**, 3499.
36 H. Chen, J. Wang, D. Shan, J. Chen, S. Zhang and X. Lu, *Anal. Chem.*, 2018, **90**, 7056.
37 Y. Wen, T. Sheng, X. Zhu, C. Zhuo, S. Su, H. Li, S. Hu, Q.-L. Zhu and X. Wu, *Adv. Mater.*, 2017, **29**, 1700778.
38 X.-G. Liu, H. Wang, B. Chen, Y. Zou, Z.-G. Gu, Z. Zhao and L. Shen, *Chem. Commun.*, 2015, **51**, 1677.
39 C.-L. Tao, Y.-M. Ying, H. Wang, B. Chen, G.-P. Zhu, Y.-J. Song, X.-G. Liu, Z. Zhao, L. Shen and B. Z. Tang, *J. Mater. Chem. C*, 2018, **6**, 12371.
40 X.-G. Liu, C.-L. Tao, H.-Q. Yu, B. Chen, Z. Liu, G.-P. Zhu, Z. Zhao, L. Shen and B. Z. Tang, *J. Mater. Chem. C*, 2018, **6**, 2983.
41 D. T. Genna, A. G. Wong-Foy, A. J. Matzger and M. S. Sanford, *J. Am. Chem. Soc.*, 2013, **135**, 10586.
42 L. Chen, R. Luque and Y. Li, *Chem. Soc. Rev.*, 2017, **46**, 4614.
43 X. Yao, X. Ma and H. Tian, *J. Mater. Chem. C*, 2014, **2**, 5155.
44 J. An, S. J. Geib and N. L. Rosi, *J. Am. Chem. Soc.*, 2009, **131**, 8376.
45 M. Gutiérrez, F. Sánchez and A. Douhal, *Phys. Chem. Chem. Phys.*, 2016, **18**, 5112.
46 X. Zhao, Y. Li, Z. Chang, L. Chen and X.-H. Bu, *Dalton Trans.*, 2016, **45**, 14888.
47 S.-S. Zhao, L. Chen, L. Wang and Z. Xie, *Chem. Commun.*, 2017, **53**, 7048.
48 J. Mei, Y. Hong, J. W. Y. Lam, A. Qin, Y. Tang and B. Z. Tang, *Adv. Mater.*, 2014, **26**, 5429.
49 H. Qu, Y. Wang, Z. Li, X. Wang, H. Fang, Z. Tian and X. Cao, *J. Am. Chem. Soc.*, 2017, **139**, 18142.
50 Z.-Q. Liu, Y. Zhao, X.-D. Zhang, Y.-S. Kang, Q.-Y. Lu, M. Azam, S. I. Al-Resayes and W.-Y. Sun, *Dalton Trans.*, 2017, **46**, 13943.
51 D. Zhao, X.-H. Liu, Y. Zhao, P. Wang, Y. Liu, M. Azam, S. I. Al-Resayes, Y. Lu and W.-Y. Sun, *J. Mater. Chem. A*, 2017, **5**, 15797.
52 Y. Zhoua, Q. Yang, D. Zhang, N. Gan, Q. Li and J. Cuan, *Sens. Actuators, B*, 2018, **262**, 137.
53 Y. Chen, K. Tsao and J. W. Keillor, *Can. J. Chem.*, 2015, **93**, 389.
54 D. Escudero, *Acc. Chem. Res.*, 2016, **49**, 1816.

